Construction and Building Materials 402 (2023) 132834

Contents lists available at ScienceDirect

Construction and Building Materials

journal homepage: www.elsevier.com/locate/conbuildmat

Delamination characterization in thin asphalt pavement structure using dispersive GPR data

Wenchao He [a], Wallace Wai-Lok Lai [a,*], Xin Sui [b], Antonios Giannopoulos [c]

[a] Department of Land Surveying and Geo-informatics, The Hong Kong Polytechnic University, Hong Kong
[b] Department of Civil and Environmental Engineering, The Hong Kong Polytechnic University, Hong Kong
[c] The School of Engineering, The University of Edinburgh, Edinburgh, EH9 3FG, UK

A B S T R A C T

Detection of delamination in asphalt pavement by non-destructive ground penetrating radar (GPR) is useful for effective maintenance and repair. However, limitations of GPR survey resolution and multiple wave interferences have made thin delamination layer characterization a challenging task in conventional common offset profiling (COP) mode. In this paper, a new method is proposed for characterizing delamination layers in asphalt pavement using the GPR waveguide dispersion model in a wide-angle reflection and refraction (WARR) configuration. The approach was validated through synthetic experiments and laboratory experiments using an asphalt pavement model. The results show that the cutoff frequencies of all modes are sensitive to air-filled delamination, while water-filled delamination leads to a significant decrease in the phase velocity of GPR waves. By observing these trends, we are able to detect delamination layers with 1 cm thickness and identify delamination layers with different properties. This new method can aid in the detection and identification of delamination layers in asphalt pavement structures.

1. Introduction

It is significant to evaluate the pavement structure to maintain its durability and extend its service life [3]. The heavy daily traffic may lead to the defects, such as cracks and delamination. For decades, a considerable body of research has focused on detecting the delamination between layers using non-destructive techniques [6,10,13]. Among these methods, ground penetrating radar (GPR) has been widely applied, which is primarily based on the propagation properties of the electromagnetic (EM) waves in the asphalt pavement structure [21,22]. Among these applications, the amplitude of the echos from the pavement is widely employed to determine the delamination boundary [20], which is generally applied with a common offset profiling (COP) configuration using GPR. In asphalt pavement, if two layers are well-constructed, the detected reflected GPR signal will be mainly determined by the dielectric properties between two such layers. When delamination occurs, a thin layer filled with air or water will generate, which will also provide a stronger echo because of the larger dielectric contrast. Such a stronger anomalous signal is expected to be detected by GPR for delamination detection. However, the resolution is limited when the wavelength of the dominant EM waves is much larger than the thin layer between two layers, which is expected because the thickness of delamination is usually less than 1 cm [8,19]. To increase the resolution, researchers developed a stepped frequency GPR system with an ultra-wideband (UWB) antenna [7]. The deconvolution and Hilbert transform have also been applied to improve the resolution [24,25,27]. In addition to the study in the time domain, information in the frequency domain has also been studied to detect the thin air-filled delamination layer [13]. Additionally in the COP mode of data collection, when the asphalt layer is thin, a shallow reflection occurs that overlaps with the direct wave. It results in interference between the two signals. This interference makes it difficult to separate the direct wave and the reflection using amplitude-based methods, which complicates the detection of delamination. To obtain extra information from multi-offset measurement, WARR mode has been applied.

In some cases, when the permittivity of the sub-layer is smaller or much bigger than the asphalt layer, the asphalt layer can act as a low-velocity or leaky waveguide and trap electromagnetic waves, where the critical angle will be reached and the total internal reflection of the GPR wave will therefore generate. The modal theory developed in previous researches[[1,2,11,12] can be used to describe the propagation of the GPR waves in the waveguide. Van der Kruk [11,12] studied the wave dispersion in such waveguides and obtained the properties and thickness of the waveguide and the half-space. The relationship between the phase velocity and frequency, which can be obtained from the phase velocity spectrum, depends on the thickness and permittivity of the waveguide layer [14]. GPR-WARR configurations were employed in previous researches to collect and analyze the guided wave, allowing the

* Corresponding author at: Department of Land Surveying and Geo-informatics, The Hong Kong Polytechnic University, Hong Kong.
E-mail address: wllai@polyu.edu.hk (W. Wai-Lok Lai).

https://doi.org/10.1016/j.conbuildmat.2023.132834
Received 12 April 2023; Received in revised form 28 July 2023; Accepted 1 August 2023
Available online 21 August 2023

Table 1
The approximate relative permittivity of asphalt pavement materials [4].

Material	Relative Permittivity, ε
Asphalt	3–5
Concrete (dry)	5–10
Air	1
Water	81

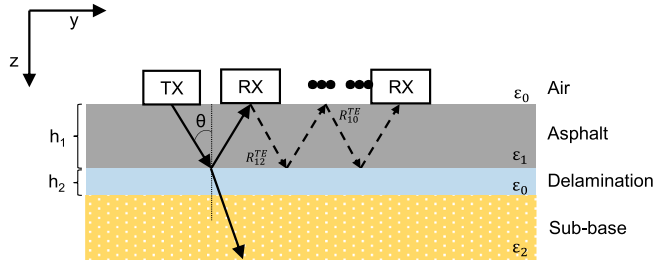

Fig. 1. Diagram of GPR detection with a wide angle reflection and refraction (WARR) antenna configuration in TE mode for EM wave propagation in an asphalt pavement model with delamination. ε_0, ε_1 and ε_2 are the real part of the permittivity of the layers. R_{ab}^{TE} is the reflection coefficient for TE mode GPR signals incident at the boundary between the a and b media.

researchers to better understand the waveguide properties.

The asphalt layer underlying a sub-layer with a higher relative permittivity will create a strong reflection at the lower interface. Total internal reflection only occurs at the upper interface beyond the critical angle in these cases. Although the lower interface is a strong reflector, some energy still transmits across it, making it a leaky waveguide. Van der Kruk et al. [16] studied an ice sheet overlying water as a leaky waveguide and estimated the permittivity and thickness of the ice sheet inversely. They found that the transverse electric (TE) mode emitted more energy into the ground than the transverse magnetic (TM) mode does. When air-filled delamination occurs between the asphalt layer and the sub-layer, the reflection index of the lower boundary changes, which alters the number of modes and shape of dispersion curves observed. As the delamination layer thickens, the asphalt waveguide shifts from a leaky waveguide to a low-velocity waveguide because asphalt has a much higher relative permittivity than air. Even when the delamination is filled with water, it remains a leaky waveguide, with the water acting as a perfect electrical reflector and the reflection coefficient of the lower interface assumed to be −1. Based on such work, the analysis was expended to evaluate the applicability of the dispersion-based method for detecting delamination in asphalt pavements using both simulated and experimental data under controlled conditions.

The flow of the proposed method is shown as follows. Firstly, the data of guided waves was collected using the GPR-WARR system and then transferred into the phase-velocity frequency domain. After that, the cutoff frequencies can be obtained from the phase-velocity spectrum, serving as a benchmark for healthy pavement structure. Then, the occurrence of delamination in the lower space of a waveguide causes changes in its dielectric permittivity, resulting in variations in the cutoff frequencies of all modes. By analyzing the changing cutoff frequencies, the presence of air and water-filled delaminations can be detected. The thickness of the air-filled delamination layer can be roughly estimated by comparing the theoretical and calculated cutoff frequency shifts. Additionally, the dispersion-based method is robust to noise [17], primarily because the multi-offset configuration in the WARR measurement acts as a filtering mechanism, effectively suppressing noise.

This paper will thus begin with a brief introduction to the modal theory, phase velocity extraction method and reflection amplitude method. Then, the results will be presented with numerical experiments based on the Finite Difference Time Domain (FDTD) method [23]. The third part will show the laboratory experiments using the multi-offset antenna on an asphalt pavement model, the results and discussion will also be given.

2. Methodology

2.1. GPR waveguide model

The approximate relative permittivities of asphalt pavement materials are shown in Table 1. Fig. 1 shows the configuration of an asphalt pavement model with delamination, where the asphalt layer acts as a leaky waveguide. The combination of the sub-layer and air or water-filled delamination layer, if any, will act as the lower space. With the occurrence of delamination and increased thickness, the dielectric properties of the sublayer will change, leading to the changing dispersion behaviour.

The fundamental equation of modal theory that describes the waveguide dispersion can be written by

$$1 - \widetilde{R}_{12}^{TE}(\theta)\widetilde{R}_{10}^{TE}(\theta)e^{-2\widetilde{\gamma}_1 h\cos(\theta)} = 0 \tag{1}$$

where ~ represents the frequency-dependent variables, $\widetilde{R}_{12}^{TE}$ and $\widetilde{R}_{10}^{TE}$ are the reflection coefficients at the lower and upper boundaries of the waveguide with an antenna in TE mode (Fig. 1). For example, $\widetilde{R}_{12}^{TE}$ is the reflection coefficient of the meida 1 (asphalt) and media 2 (sub-base). h is the thickness of the waveguide, θ is the angle of incidence and $\widetilde{\gamma}_1$ is the propagation constant defined by

$$\widetilde{\gamma}_b = \frac{j\omega\sqrt{\varepsilon_b}}{c_0} \tag{2}$$

where ε_b is the real part of the permittivity of layer b, and $c_0 = 2.9998 \times 10^8$ m/s is the speed of light in the vacuum. In the cases where a low-velocity layer is sandwiched by two high-velocity layers, two requirements are needed to solve Eq. (1). First, the two reflection coefficients must have a unit amplitude such that the EM waves will totally reflect at both upper and lower boundaries. For the wave propagating in the waveguide, the total reflection will first occur at the upper interface and then at the lower interface, in which the following two conditions are fulfilled. First, the critical angle of the lower boundary must follow the Snell's Law:

$$\theta_{12}^{c} = sin^{-1}\left(\sqrt{\frac{\varepsilon_2}{\varepsilon_1}}\right). \tag{3}$$

Second, the total phase change (after reflection at upper and lower interfaces) must be equal to $2m\pi$ radians, with an integer m. Substituting Eq. (2) in Eq. (1) yields

$$\widetilde{\phi}(\theta) - \frac{4\pi f\sqrt{\varepsilon_1}h\cos(\theta)}{c_0} = -2m\pi \tag{4}$$

where

$$\widetilde{\phi}(\theta) = tan^{-1}\left[\frac{Im\left(\widetilde{R}_{10}\right)}{Re\left(\widetilde{R}_{10}\right)}\right] + tan^{-1}\left[\frac{Im\left(\widetilde{R}_{12}\right)}{Re\left(\widetilde{R}_{12}\right)}\right]. \tag{5}$$

The variation of m corresponds to different guided-wave modes. For fundamental mode, $m = 0$. It shall be noted that this derivation works in lossless conditions without material dispersion which is presuming the case in the GPR plateau [5].

The cutoff frequency describes the lowest frequency at which a guided wave can propagate through the waveguide. For asymmetric waveguides (i.e., dielectric permittivities are different between either side of the waveguide), the cutoff frequency can be determined by rewriting Eq. (4) as:

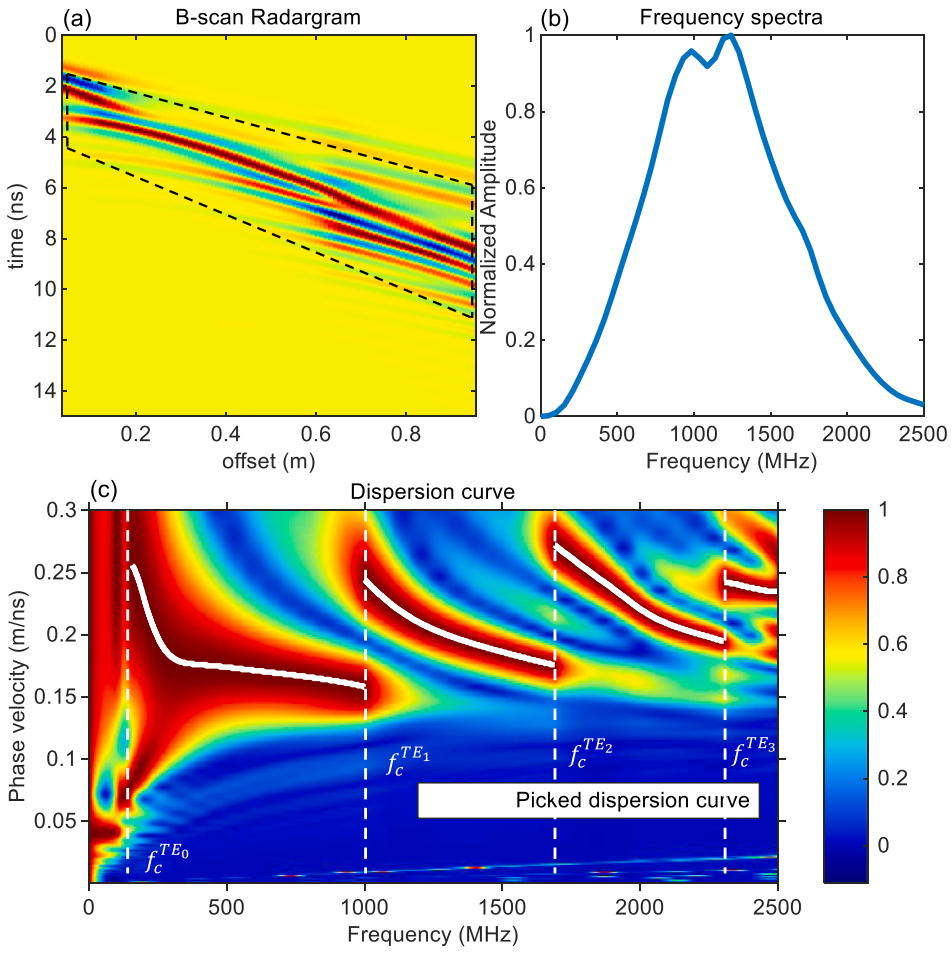

Fig. 2. The typical (a) WARR radargram, (b) frequency spectrum and (c) phase velocity spectrum. The solid white lines in (c) represent the optimal phase velocities for each frequency component, and the vertical white dashed lines show the cutoff frequencies.

$$f_m = \frac{\left[2\pi m + \widetilde{\phi}(\theta)\right] c_0}{4\pi\sqrt{\varepsilon_1} h cos(\theta)} \tag{6}$$

where θ will be evaluated as θ_{12}^c (Eq. (3)). Based on the reflection theory, the reflection coefficients for this total reflection angle are given by

$$R_{10}(\theta_{12}^c) = \frac{\varepsilon_0 + \varepsilon_1 - 2\varepsilon_2 + 2i\sqrt{\varepsilon_1 - \varepsilon_2}\sqrt{\varepsilon_2 - \varepsilon_0}}{\varepsilon_1 - \varepsilon_0} \tag{7}$$

$$R_{12}(\theta_{12}^c) = 1 \tag{8}$$

Substituting Eq. (7) and Eq. (8) in Eq. (5) yields

$$\phi(\theta_{12}^c) = tan^{-1}\left(\frac{2\sqrt{\varepsilon_1 - \varepsilon_2}\sqrt{\varepsilon_2 - \varepsilon_0}}{\varepsilon_0 + \varepsilon_1 - 2\varepsilon_2}\right). \tag{9}$$

When water-filled delamination occurs, the total reflection still occurs at the upper interface beyond the critical angle θ_c, where

$$\theta_c = sin^{-1}\left(\sqrt{\frac{\varepsilon_0}{\varepsilon_1}}\right). \tag{10}$$

The water can be considered a perfect reflector, where an approximation $\widetilde{R}_{12} = -1$ can then be assumed. Substitution of $\widetilde{R}_{12} = -1$ and Eq. (10) into Eq. (1) gives the expressions of the cutoff frequencies of a leaky waveguide:

$$f_m = \frac{(2m+1)c_0}{4h\sqrt{\varepsilon_1 - 1}} \tag{11}$$

In addition to the scenarios described above, there are cases in which the permittivity of the half-space is greater than that of the waveguide, but the half-space cannot be considered a perfect electric conductor (PEC). An example of such a scenario is when asphalt with a permittivity of 5 overlies a concrete sub-layer with a permittivity of 10. In such cases, it is difficult to calculate the cutoff frequency using the conventional formula. However, it can still be obtained from the phase-velocity spectrum, which provides a solution in these complex cases.

2.2. Phase velocity extraction from WARR data

The phase shift method developed by Park [15] is employed for extracting the phase velocity dispersion curve in this paper. First, the WARR data $X(x,t)$ are transformed into the frequency domain:

$$\widehat{X}(x,f) = \int X(x,t)e^{-2\pi fti}dt. \tag{12}$$

Each frequency component $\widehat{X}(x,f)$ has an amplitude $|\widehat{X}(x,f)|$ and phase $\phi(x,f)$. For a frequency component f_i with a phase velocity v_i, its phase change is a function of offset change Δx, given by

$$\Delta\phi = -\frac{2\pi f_i}{v_i}\Delta x. \tag{13}$$

Inversing the phase change given by Eq. (13) to the normalized frequency components and summing the results over all offsets of the WARR data give the phase velocity spectrum $U(v,f)$

$$U(v,f) = \left|\sum_x \frac{\widehat{X}(x,f)}{|\widehat{X}(x,f)|} e^{\frac{2\pi fxi}{v}}\right|. \tag{14}$$

Table 2
The input parameters of the simulation models.

	ε	σ_{dc}(S/m)	h(cm)
Air-filled layer	1	0	0–5
Water-filled layer	81	0.01	0.5, 2
Asphalt	5	0.0001	10
Sub-base	10	0.001	–

The largest amplitude in the phase spectrum represents the optimal estimation of the phase velocity for each frequency component, defined as

$$v_{optimal}(f_i) = \max[U(v,f_i)]. \quad (15)$$

Fig. 2 shows a typical WARR radargram and the corresponding frequency and phase velocity spectrum. The GPR data selected for dispersion curve extraction are represented by the area highlighted by the black dashed lines in Fig. 2(a). The white solid lines in Fig. 2(c) depict the optimal phase velocity curves, while the white dashed lines in the same figure indicate the cutoff frequencies of different modes.

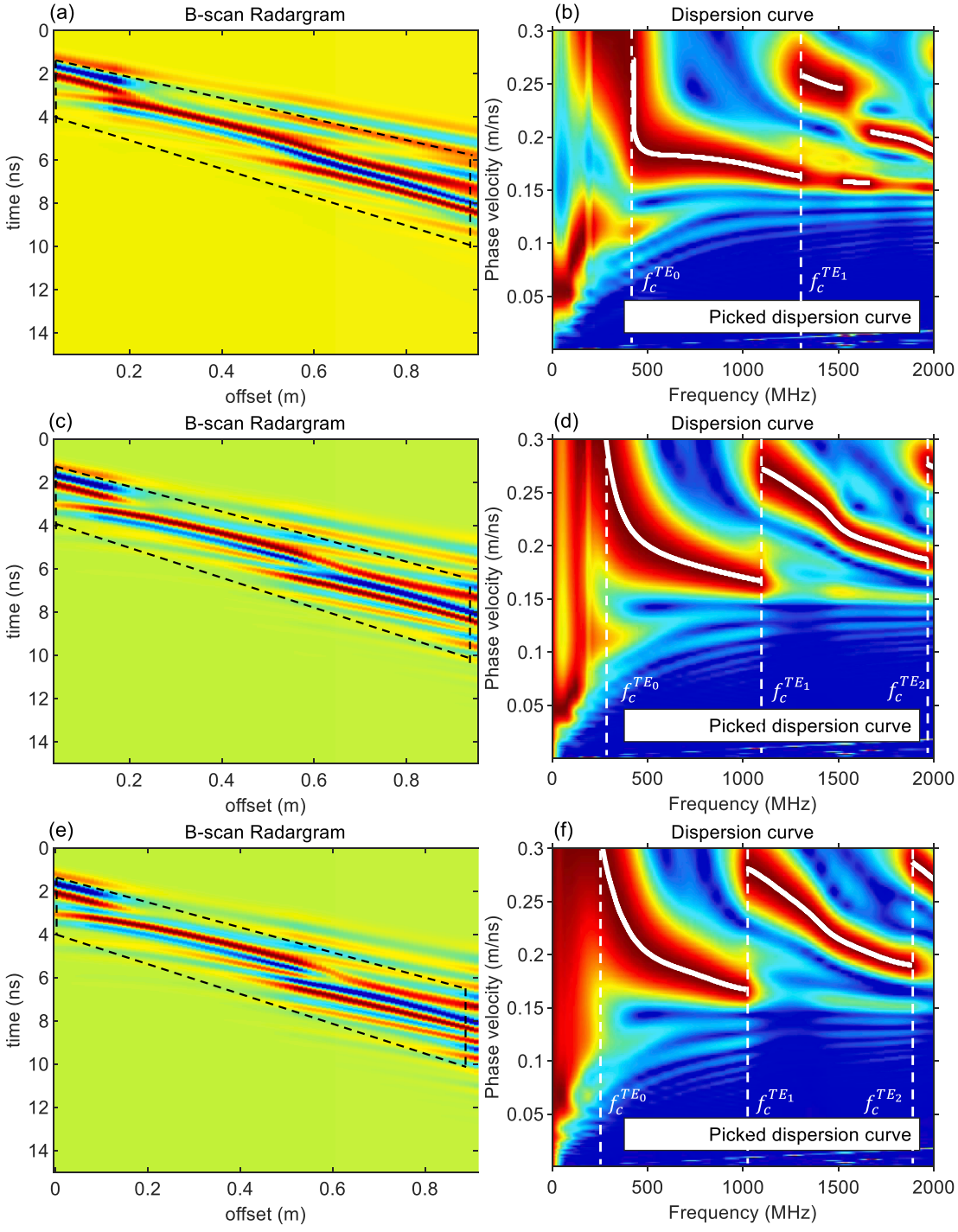

Fig. 3. WARR radargrams and the corresponding dispersion spectra with the air gap thickness of 0 cm (a,b), 0.5 cm (c,d) and 2 cm (e,f).

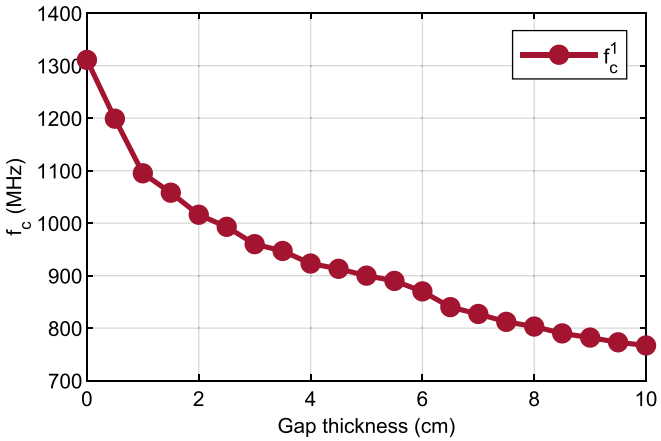

Fig. 4. The picked cutoff frequencies of the first mode verse the air gap thickness.

3. Experiments and results

3.1. Simulation experiments

A series of numerical experiments were conducted using GPRMax [9,23], an open-source Finite-Difference Time-Domain method (FDTD) simulation software that allows users to simulate the GPR response to the subsurface world. To validate the proposed method, we established different simulation models that correspond to the scenarios discussed in section 2.1. The models differed in their relative permittivities and were designed to provide insights into the behaviour of the two-layer asphalt pavement model under different delamination conditions. The general model had relative permittivities of 5 and 10 for the waveguide and lower space, respectively. To simulate air- and water-filled delamination, the relative permittivities of 1 and 81 were used, respectively. The TE mode was selected for all experiments and used a Ricker wavelet with a centre frequency of 900 MHz for excitation. The time window was set to 15 ns with a step interval of 0.01 cm. Table 2 presents the model parameters in detail. By conducting these experiments, we were able to gain a better understanding of the behaviour of the pavement model and validate the effectiveness of the proposed method.

Fig. 3 displays some of the results of the simulation, which demonstrate the dispersive nature of all the WARR data. The dispersive data are indicated by the black dashed lines. Fig. 3(a,b) shows the results of the model simulating the healthy structure, where the cutoff frequency of the first mode is around 1310 MHz. Notably, there is a clear reduction in the cutoff frequencies of all modes as the delamination occurs and thickens, as shown in Fig. 3(b, d, f).

Based on the frequency spectrum shown in Fig. 1, the effective bandwidth was determined approximately between 300 and 2100 MHz when a threshold of 15% of the maximum amplitude was used. This bandwidth was used in the following analysis of the cutoff frequencies. The first cutoff frequencies were focused, as they are most suitable for studying delamination due to their proximity to the strongest signal amplitude. As shown in Fig. 4, the cutoff frequencies of the first mode exhibit a two-stage trend. In the first stage, the cutoff frequencies of the first mode decrease sharply from 1310 MHz to 1100 MHz as the gap

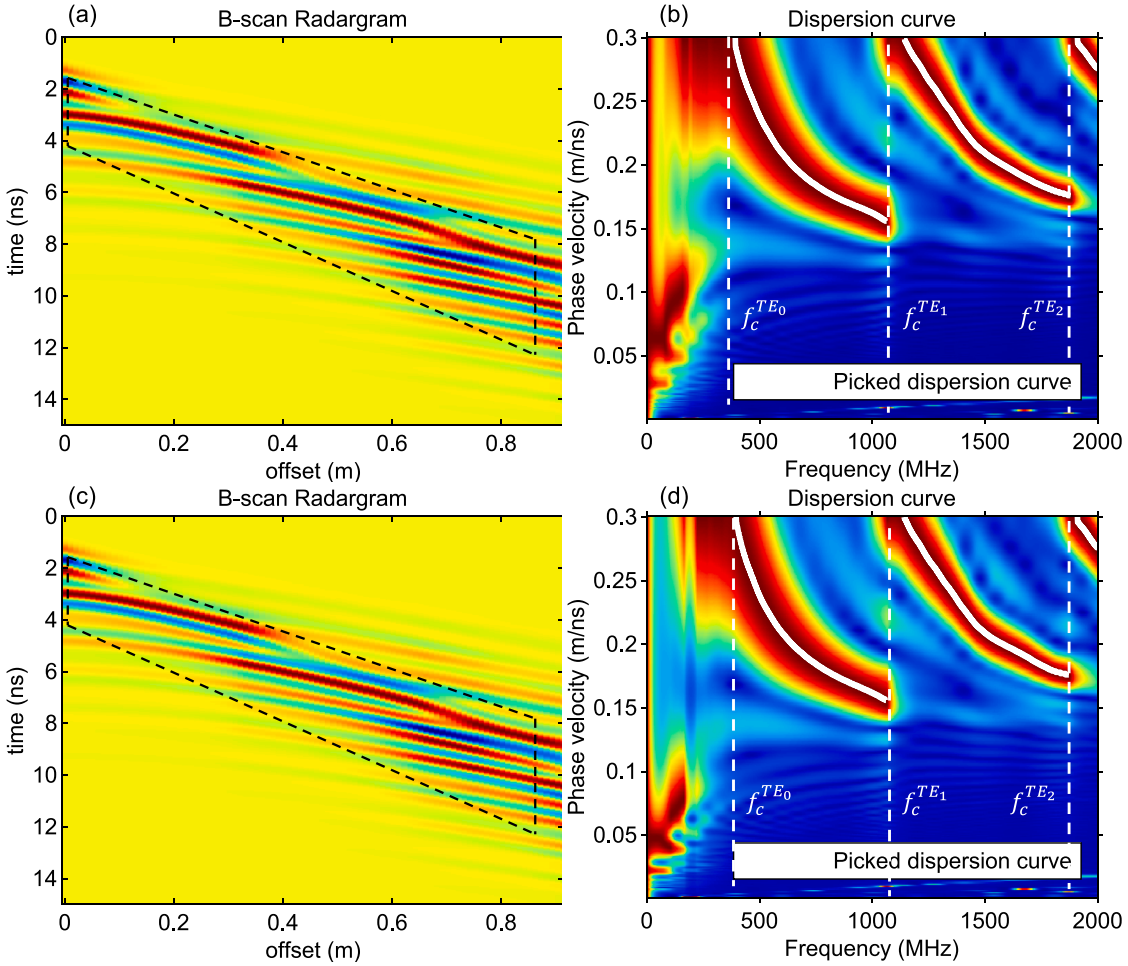

Fig. 5. WARR radargrams and the corresponding dispersion spectra with the water gap thickness of 0.5 cm (a, b) and 2 cm (c, d).

Fig. 6. Laboratory GPR measurement setup.

thickness increases from 0 cm to 1 cm. In the second stage, there is a slight decrease by 440 MHz in the first mode cutoff frequencies as gap thickness increases from 1 cm to 10 cm.

The decreases of the cutoff frequencies in all modes with increasing air gap thickness can be explained by the modal theory introduced in Section 2.1. Specifically, it is found that the occurrence of air-filled delamination causes a change in the dielectric properties of the lower layer. The relative permittivity of the lower layer decreases from that of the concrete (10) to air (1), and this decrease is not linear. When the thickness of the delamination is comparable to the wavelength of the dominant GPR wave propagating in the waveguide, the air-filled delamination can be seen as a new lower layer. Therefore, the dielectric properties of the new lower layer and upper layer are the same, where $\varepsilon_2 = \varepsilon_0$. The critical angles at the two interfaces are equal, and the reflection coefficients $R_{10}(\theta_{12}^c) = 1$, and the equation expressing the cutoff frequency given in Eq. (6) can be written as

$$f_c^m = \frac{mc_0}{2h\sqrt{\varepsilon_1 - \varepsilon_2}}. \tag{16}$$

As can be seen in Fig. 4, as the delamination thickness increases, the cutoff frequencies of the first mode gradually decrease to 760 MHz, which is almost equal to the cutoff frequency of the first mode when the asphalt layer is sandwiched by air, 750 MHz.

Due to the dispersion of GPR data (Fig. 3a,c,e), it is difficult to pick a travel time for a GPR reflection, limiting the use of travel-time analysis methods. The dispersion-based method was proposed to address this issue, and simulation results indicate that the air-filled delamination with a thickness ranging from 0.5 cm to 10 cm can be detected using this method, which is much smaller than $\lambda_d/8$, where λ_d is the wavelength of the GPR wave. Based on Eq. (16), we can roughly estimate the thickness of the air-filled delamination when it is comparable to the wavelength of GPR. The cutoff frequency of the first mode is recommended as an index to detect delamination since it is commonly one of the strongest components of the transmitted wave, while the cutoff frequencies of higher modes are more sensitive to changes in the dielectric properties of the lower layer but are weaker in intensity and thus more susceptible to noise interference.

The results of water-filled delamination simulation models (Fig. 5) show that the cutoff frequencies of all modes decrease significantly compared to those without delamination. In comparison to air-filled delamination, the cutoff frequency of the fundamental mode can be used as an index to identify the delamination material, as it decreases substantially with increasing air-filled delamination thickness. However, the cutoff frequency of the fundamental mode changes only slightly with water-filled delamination.

Regarding the gap thickness, the lower space's permittivities have little influence on the cutoff frequencies once a water-filled gap occurs, meaning that the cutoff frequencies of different modes will not change with varying water-filled delamination thickness. Simulation results (Fig. 5) of water-filled delamination with 0.5 and 2 cm thickness agree well with the results calculated by Eq. (11), where the cutoff frequencies of the foundational, first, and second modes are almost the same at 381, 1124, and 1879 MHz, respectively.

3.2. Laboratory experiments

To validate the findings of the simulation experiments, laboratory experiments were conducted using a GPR system manufactured by Geophysical Survey Systems, Inc. (GSSI). The experimental setup is shown in Fig. 6, which consists of two new asphalt layers with a thickness of 5 cm placed on top of the wet sand with a thickness of 90 cm. A pair of 900 MHz antennas with a SIR-30 control unit is employed. Delaminations filled with air and water are present between the asphalt layer and the sand. Four sets of tests were conducted with air gap thicknesses of 0 cm, 1 cm, 2 cm, and 3 cm, and a saturated cotton cloth was used to simulate water-filled delamination with a thickness of 0.5 cm.

The GSSI 2 GHz palm GPR was employed to estimate the permittivity of the asphalt using the surface amplitude reflection method [26]. The group velocity of the wet sand obtained from the GPR-WARR measurement was used to estimate the permittivity of the wet sand, and the estimated results served as the benchmark. The estimated permittivities of the asphalt and sand are 4.88 and 9.3, respectively. The average thickness of the two-layers asphalt structure is 10 cm, the same as the value measured by tape.

The outcomes of the laboratory experiments, conducted with varying air gap thicknesses, are illustrated in Fig. 7. The phase-velocity dispersion spectra exhibit characteristics analogous to those observed in the simulation results. A notable decrease in the cutoff frequencies of the first mode is observed with the emergence of delamination and increases in air gap thicknesses. Given the importance of amplitude quality, this paper will focus exclusively on the analysis of the first mode's cutoff frequencies.

Fig. 8 displays the cutoff frequencies for varying air-filled delamination thicknesses. The results demonstrate that the cutoff frequencies of the first mode decrease with increasing air-filled delamination thickness. The relationship between the cutoff frequencies and gap thickness is in good agreement with the numerical results from the first stage, providing evidence that the detection of delamination occurring between the thin asphalt layer and the sub-layer is possible based on the decreasing cutoff frequencies.

Fig. 9 displays the results of the water-filled delamination detection. Different from the air-fill delamination, the cutoff frequencies of the fundamental and first modes of water-fill delamination results are

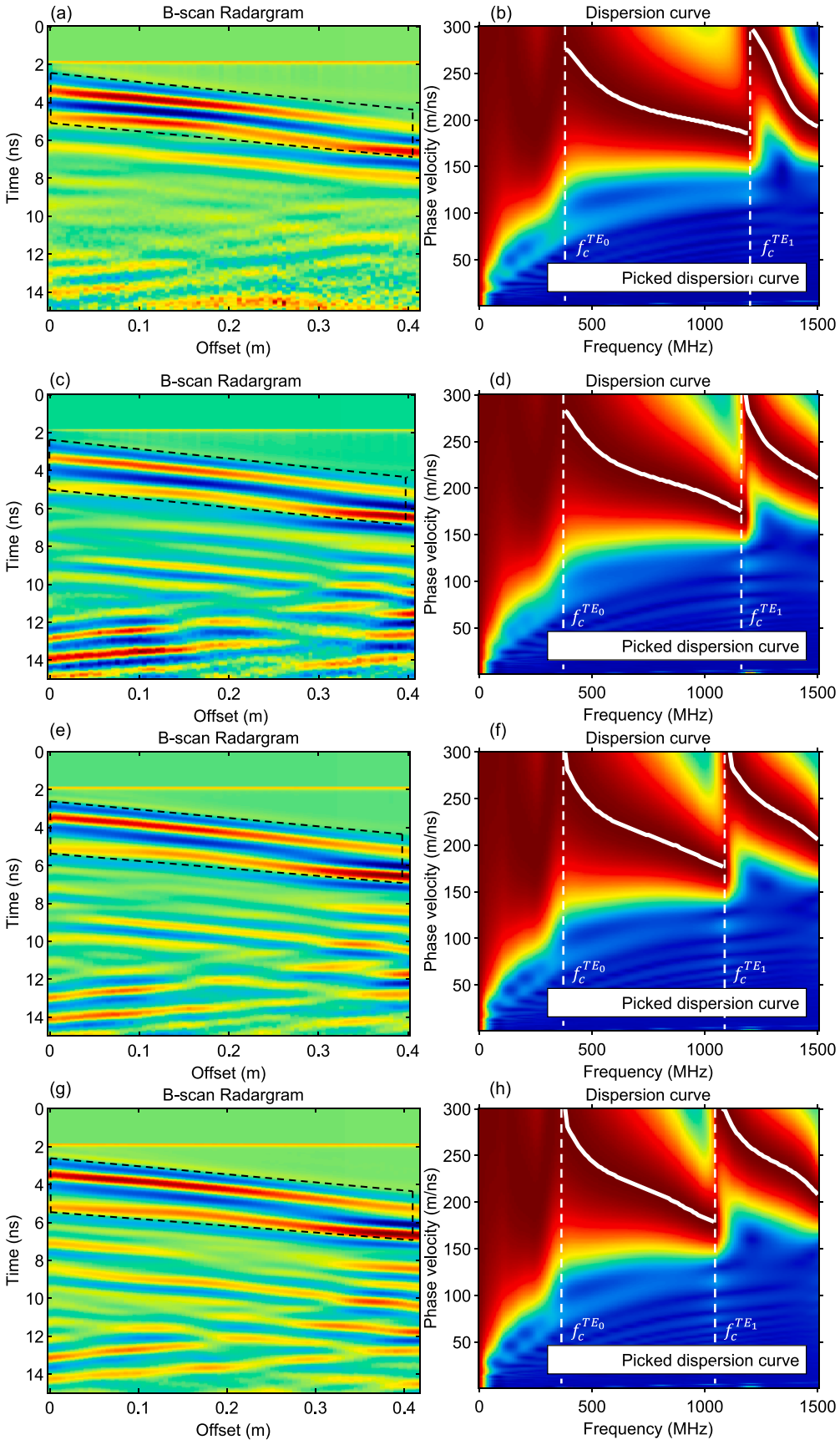

Fig. 7. WARR radargrams and the corresponding dispersion spectra with the air gap thickness of 0 cm (a,b), 0.5 cm (c,d), 2 cm (e,f) and 3 cm (j.h).

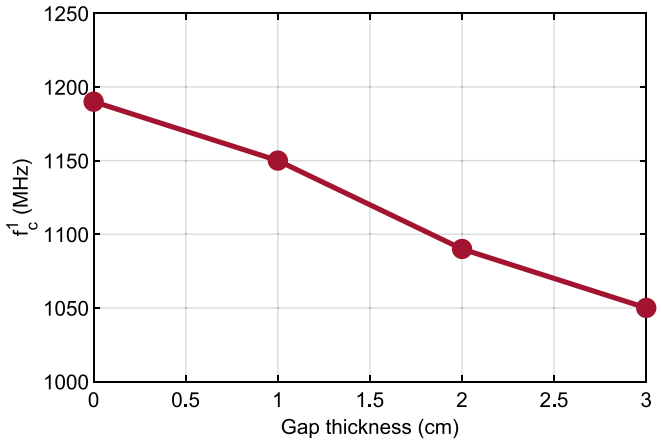

Fig. 8. The picked cutoff frequencies of the first mode verse the gap thickness from laboratory data.

similar to those of results without delamination. However, large decreases in phase velocities of all modes can still help us detect the water-filled delamination and identify the material of the delamination. The different dielectric properties of the materials used to create the filling water delamination in the simulation and laboratory experiments resulted in different outcomes. In the simulation experiment, pure water with a dielectric constant of 81 was used, whereas, in the laboratory experiment, saturated cotton cloth was used to simulate the water-filled delamination. The cotton cloth is not a PEC, but its higher dielectric constant compared to the asphalt layer still affects the phase velocity of GPR waves, resulting in a decrease of the phase velocity [16,18]. This effect can help detect the delamination and identify the material of the delamination.

4. Conclusion

In this paper, a novel method was proposed for detecting air-filled delamination in asphalt pavement structures using dispersive GPR data. The method involves GPR data collection in WARR configuration, followed by transforming the data from the time-spatial domain into the phase-velocity frequency domain, and picking the optimal dispersion curve and the cutoff frequencies of different modes.

To validate the proposed approach, numerical experiments were conducted on an asphalt pavement model with varying air and water-filled delamination thicknesses, as well as laboratory experiments on a two-layers asphalt pavement model. Both experiments showed that compared to the healthy structure baseline, the cutoff frequencies of different modes decreased as the air gap thickness increased. The decrease occurred mainly in the first stage, where the gap thickness was 0–1 cm, and became less apparent when the gap thickness was larger than 1 cm. This small scale of measurement is impossible in traditional GPR COP mode of survey

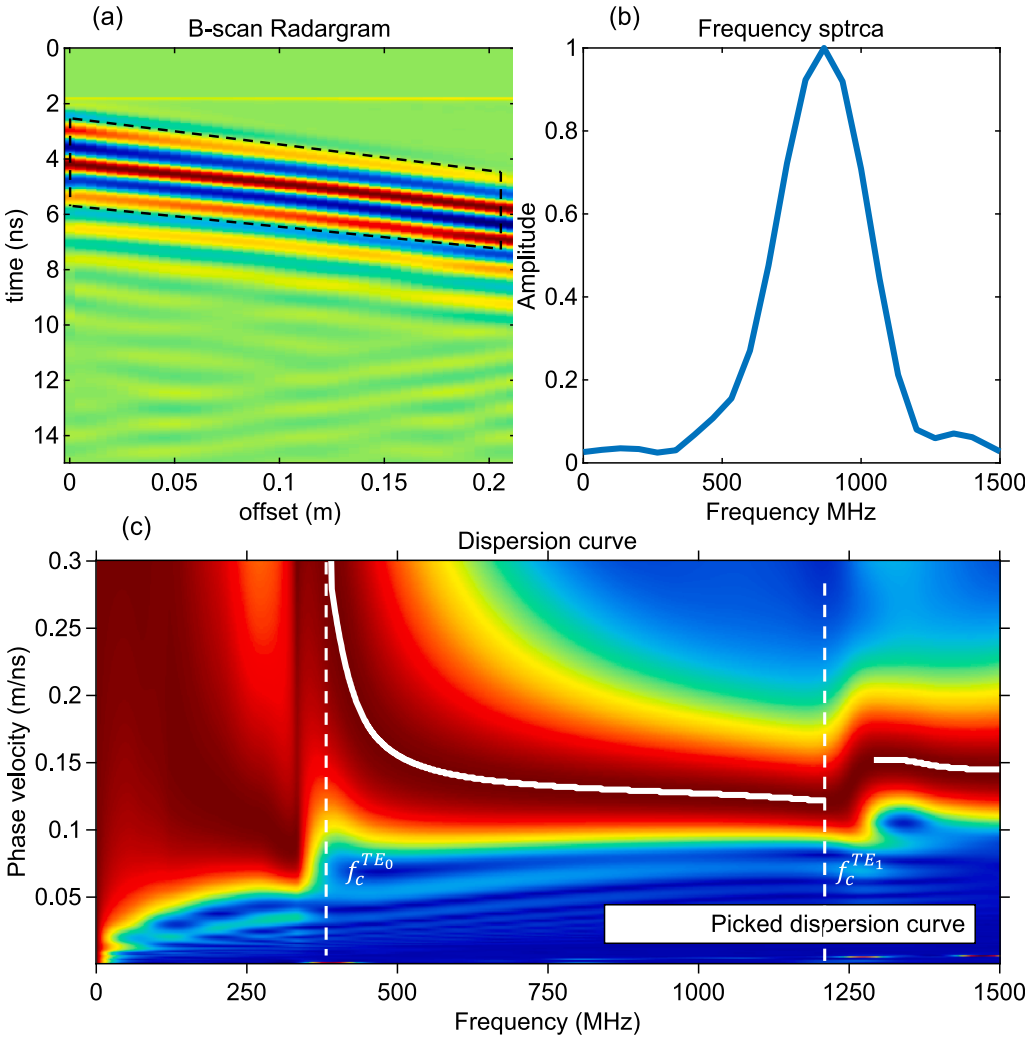

Fig. 9. The (a) WARR radargram, (b) frequency spectrum and (c) phase velocity spectrum of the asphalt pavement model with water-filled delamination.

Moreover, it was found that the large decrease in phase velocity resulting from the water-filled delamination can help detect the delamination and identify the materials of the delamination. Therefore, based on the cutoff frequency and phase velocity shifts, the proposed method can accurately detect the presence and materials of delamination in asphalt structures. Using the cutoff frequency of the first mode as the index is recommended because of its better amplitude quality than the higher modes.

Overall, our proposed method has demonstrated great potential in the non-destructive evaluation of asphalt pavement structures, providing a valuable contribution to the field of civil engineering.

CRediT authorship contribution statement

Wenchao He: Conceptualization, Data curation, Formal analysis, Investigation, Methodology, Software, Writing – original draft. **Wallace Wai-Lok Lai:** Project administration, Supervision, Writing – review & editing. **Xin Sui:** Data curation, Investigation. **Antonios Giannopoulos:** Supervision, Writing – review & editing.

Declaration of Competing Interest

The authors declare that they have no known competing financial interests or personal relationships that could have appeared to influence the work reported in this paper.

Data availability

Data will be made available on request.

Acknowledgement

The funding support by the Research Grants Council of the Hong Kong University Grants Committee on the projects “Waveguide Characterization of Shallow Subsurface Damages in Infrastructure Materials by Dispersive Behavior of Ground Penetrating Radar Wave” [PolyU 15216619] and ‘Time-lapse Imaging and Diagnosis of Urban Subsurface Hazards by Ground Penetrating Radar’ [PolyU 15204320] are gratefully acknowledged.

References

[1] S.A. Arcone, Field observations of electromagnetic pulse propagation in dielectric slabs, Geophysics 49 (10) (1984) 1763–1773.
[2] S.A. Arcone, P.R. Peapples, L. Liu, Propagation of a ground-penetrating radar (GPR) pulse in a thin-surface waveguide, Geophysics 68 (6) (2003) 1922–1933.
[3] V. Baltazart, J.M. Moliard, R. Amhaz, L.M. Cottineau, A. Wright, D. Wright, M. Jethwa, Automatic Crack Detection on Pavement Images for Monitoring Road Surface Conditions—Some Results from the Collaborative FP7 TRIMM Project, in: A. Chabot, W.G. Buttlar, E.V. Dave, C. Petit, G. Tebaldi (Eds.), 8th RILEM International Conference on Mechanisms of Cracking and Debonding in Pavements, Springer, Netherlands, Dordrecht, 2016, pp. 719–724.
[4] D6432-19, A., 2020. Standard Guide for Using the Surface Ground Penetrating Radar Method for Subsurface Investigation.
[5] J.L. Davis, A.P. Annan, Ground-penetrating radar for high-resolution mapping of soil and rock stratigraphy1, Geophysical Prospecting 37 (5) (1989) 531–551.
[6] X. Dérobert, V. Baltazart, J.-M. Simonin, S.S. Todkar, C. Norgeot, H.-Y. Hui, GPR monitoring of artificial debonded pavement structures throughout its life cycle during accelerated pavement testing, Remote Sensing 13 (8) (2021) 1474.
[7] X. Dérobert, C. Fauchard, P.h. Côte, E. Le Brusq, E. Guillanton, J.Y. Dauvignac, C. h. Pichot, Step-frequency radar applied on thin road layers, J. Appl. Geophys. 47 (3-4) (2001) 317–325.
[8] Z. Dong, S. Ye, Y. Gao, G. Fang, X. Zhang, Z. Xue, T. Zhang, Rapid detection methods for asphalt pavement thicknesses and defects by a vehicle-mounted ground penetrating radar (gpr) system, Sensors 16 (12) (2016) 2067.
[9] A. Giannopoulos, Modelling ground penetrating radar by GprMax, Constr. Build. Mater. 19 (10) (2005) 755–762.
[10] V.H.Y. Hui, X. Dérobert, W.W.L. Lai, A study of artificial debond pavement under controlled traffic by Ground Penetrating Radar, J. Appl. Geophys. 204 (2022), 104722.
[11] J.v.d. Kruk, Properties of surface waveguides derived from inversion of fundamental and higher mode dispersive GPR data, IEEE Trans. Geosci. Remote Sensing 44 (2006) 2908–2915.
[12] J.V.D. Kruk, R. Streich, A.G. Green, Properties of surface waveguides derived from separate and joint inversion of dispersive TE and TM GPR data, Geophysics 71 (1) (2006) K19–K29.
[13] H. Liu, Z. Deng, F. Han, Y. Xia, Q.H. Liu, M. Sato, Time-frequency analysis of air-coupled GPR data for identification of delamination between pavement layers, Constr. Build. Mater. 154 (2017) 1207–1215.
[14] A.R. Mangel, S.M.J. Moysey, J. van der Kruk, Resolving precipitation induced water content profiles by inversion of dispersive GPR data: a numerical study, J. Hydrol. 525 (2015) 496–505.
[15] C.B. Park, R.D. Miller, J. Xia, Imaging dispersion curves of surface waves on multi? channel record, seg technical program expanded abstracts 1998, Soc. Exploration Geophys. (1998) 1377–1380.
[16] J. van der Kruk, S.A. Arcone, L. Liu, Fundamental and higher mode inversion of dispersed GPR waves propagating in an ice layer, IEEE Trans. Geosci. REMOTE Sensing 45 (2007) 2483–2491.
[17] J. van der Kruk, N. Diamanti, A. Giannopoulos, H. Vereecken, Inversion of dispersive GPR pulse propagation in waveguides with heterogeneities and rough and dipping interfaces, J. Appl. Geophys. 81 (2012) 88–96.
[18] J. van der Kruk, C.M. Steelman, A.L. Endres, H. Vereecken, Dispersion inversion of electromagnetic pulse propagation within freezing and thawing soil waveguides, Geophys. Res. Lett. 36 (18) (2009).
[19] Van der Wielen, A., 2014. Characterization of thin layers into concrete with Ground Penetrating Radar.
[20] W. Wai-Lok Lai, X. Dérobert, P. Annan, A review of ground penetrating radar application in civil engineering: a 30-year journey from locating and testing to imaging and diagnosis, NDT & E Int. 96 (2018) 58–78.
[21] S. Wang, Z. Leng, Z. Zhang, X. Sui, Automatic asphalt layer interface detection and thickness determination from ground-penetrating radar data, Constr. Build. Mater. 357 (2022), 129434.
[22] S. Wang, X. Sui, Z. Leng, J. Jiang, G. Lu, Asphalt pavement density measurement using non-destructive testing methods: current practices, challenges, and future vision, Constr. Build. Mater. 344 (2022), 128154.
[23] C. Warren, A. Giannopoulos, I. Giannakis, gprMax: open source software to simulate electromagnetic wave propagation for Ground Penetrating Radar, Computer Phys. Commun. 209 (2016) 163–170.
[24] J. Xia, E. Franseen, R. Miller, T. Weis, Application of deterministic deconvolution of ground-penetrating radar data in a study of carbonate strata, J. Appl. Geophys. 56 (3) (2004) 213–229.
[25] Z.H.A.N.G. Xian-Wu, G.Y.-Z. FANG Guang-You, Application of Hilbert spectrum analysis in Ground Penetrating Radar thin layer recognition, Chin. J. Geophys. 56 (2013) 2790–2798.
[26] S. Zhao, I.L. Al-Qadi, S. Wang, Prediction of thin asphalt concrete overlay thickness and density using nonlinear optimization of GPR data, NDT & E Int. 100 (2018) 20–30.
[27] S. Zhao, P. Shangguan, I.L. Al-Qadi, Application of regularized deconvolution technique for predicting pavement thin layer thicknesses from ground penetrating radar data, NDT & E Int. 73 (2015) 1–7.